Received: 8 March 2018 | Revised: 5 December 2018 | Accepted: 13 February 2019

DOI: 10.1002/term.2824

RESEARCH ARTICLE

WILEY

Non-destructive detection of matrix stabilization correlates with enhanced mechanical properties of self-assembled articular cartilage

Anne K. Haudenschild[1] | Benjamin E. Sherlock[1] | Xiangnan Zhou[1] | Jerry C. Hu[2] | J. Kent Leach[1,3] | Laura Marcu[1]* | Kyriacos A. Athanasiou[2]*

[1] Department of Biomedical Engineering, University of California Davis, Davis, CA, USA

[2] Department of Biomedical Engineering, University of California Irvine, Irvine, CA, USA

[3] Department of Orthopaedic Surgery, University of California Davis Medical Center, Sacramento, CA, USA

Correspondence
Kyriacos A. Athanasiou, Department of Biomedical Engineering, University of California Irvine, 3120 Natural Sciences II, Irvine, CA 92697-2715, USA.
Email: athens@uci.edu

Funding information
National Institutes of Health, Grant/Award Number: R01AR067821; California Institute for Regenerative Medicine, Grant/Award Number: RT3-07981

Abstract

Tissue engineers rely on expensive, time-consuming, and destructive techniques to monitor the composition, microstructure, and function of engineered tissue equivalents. A non-destructive solution to monitor tissue quality and maturation would greatly reduce costs and accelerate the development of tissue-engineered products. The objectives of this study were to (a) determine whether matrix stabilization with exogenous lysyl oxidase-like protein-2 (LOXL2) with recombinant hyaluronan and proteoglycan link protein-1 (LINK) would result in increased compressive and tensile properties in self-assembled articular cartilage constructs, (b) evaluate whether label-free, non-destructive fluorescence lifetime imaging (FLIm) could be used to infer changes in both biochemical composition and biomechanical properties, (c) form quantitative relationships between destructive and non-destructive measurements to determine whether the strength of these correlations is sufficient to replace destructive testing methods, and (d) determine whether support vector machine (SVM) learning can predict LOXL2-induced collagen crosslinking. The combination of exogenous LOXL2 and LINK proteins created a synergistic 4.9-fold increase in collagen crosslinking density and an 8.3-fold increase in tensile strength as compared with control (CTL). Compressive relaxation modulus was increased 5.9-fold with addition of LOXL2 and 3.4-fold with combined treatments over CTL. FLIm parameters had strong and significant correlations with tensile properties (R^2 = 0.82; p < 0.001) and compressive properties (R^2 = 0.59; p < 0.001). SVM learning based on FLIm-derived parameters was capable of automating tissue maturation assessment with a discriminant ability of 98.4%. These results showed marked improvements in mechanical properties with matrix stabilization and suggest that FLIm-based tools have great potential for the non-destructive assessment of tissue-engineered cartilage.

KEYWORDS

autofluorescence, biomechanics, cartilage, imaging, non-destructive monitoring, tissue engineering

*Athanasiou and Marcu should be considered joint senior authors.

1 | INTRODUCTION

The tissue engineering and regenerative medicine industries have an immense potential to improve the clinical outcome and deliver effective curative therapies to a number of chronic diseases that are currently beyond repair. The U.S. Food and Drug Administration (FDA) has outlined a series of guidance documents for the clinical application of tissue-engineered products that specify thorough characterization during the development and manufacturing process and defined acceptance criteria for product release (FDA, 2011). In current practice, tissue engineers rely on a battery of expensive, time-consuming, and destructive techniques to monitor the composition, microstructure, and function of engineered tissue equivalents. A non-destructive solution to monitor tissue quality and maturation would address the significant hurdles that these new regulations pose for the translation of cell-based tissue products into the clinic, greatly reduce costs, speed the development of tissue products, and allow clinical evaluation of current and emerging therapeutic interventions.

Quantitative optical techniques based on endogenous tissue autofluorescence have been developed to image and non-destructively characterize tissue properties (Gorpas et al., 2015; Gorpas, Ma, Bec, Yankelevich, & Marcu, 2016; M. Y. Sun et al., 2012). A number of endogenous biomolecules, including the extracellular matrix protein collagen (Alfonso-Garcia, Haudenschild, & Marcu, 2018) and its crosslinks (Wagnieres, Star, & Wilson, 1998), and proteoglycans (Angheloiu et al., 2011) give rise to tissue autofluorescence. The relative concentration and distribution of individual fluorophores within the tissue create unique fluorescence emission profiles that can be quantified. Fluorescence lifetime imaging (FLIm) utilizes the exponential decay rate of these endogenous fluorophores, termed the fluorescence lifetime (LT), to generate images of tissue biochemistry and can be implemented in a single, narrow, and flexible fiber optic interface between the apparatus and the sample (Marcu, French, & Elson, 2014). Fiber-based, FLIm has been used to detect native cartilage matrix depletion and correlated with changes in mechanical properties (Haudenschild et al., 2018). Data processing techniques have been developed to allow near real-time acquisition (Marcu et al., 2014) and quantification (Liu, Sun, Qi, & Marcu, 2012) of FLIm parameters to detect biochemical changes in various biological tissues, both *in vitro* and *in vivo* (Fite et al., 2011; Manning et al., 2013; Yankelevich et al., 2014).

In addition to monitoring the changes in biochemical composition during tissue development and maturation, it is also necessary to quantify changes in the mechanical properties of both native and engineered replacement tissues to determine successful tissue functionality. Articular cartilage is a load-bearing tissue composed of primarily collagen type II, proteoglycans, and water (Zhang, Hu, & Athanasiou, 2009), where there is a direct structure–function relationship between the mechanical properties and the biochemical composition of the tissue (Setton, Mow, Muller, Pita, & Howell, 1993; Figure 1 a). Articular cartilage compressive properties are strongly associated with proteoglycan content. Hyaluronan and proteoglycan link protein-1 (LINK) is a glycoprotein that stabilizes the interaction between the major proteoglycan structural components, aggrecan and hyaluronic acid (Hardingham, 1979; Seyfried et al., 2005), creating large, negatively charged aggregates. The resulting LINK-stabilized aggregates imbibe water and provide cartilage with its osmotic properties, which are critical to its ability to resist compressive loads (Kiani, Chen, Wu, Albert, & Burton, 2002; Z. Wang, Weitzmann, Sangadala, Hutton, & Yoon, 2013). Articular cartilage tensile properties are strongly associated with collagen and collagen crosslinking content. Despite recent advances, tissue-engineered cartilage currently lacks the mechanical strength of native tissue (Huey, Hu, & Athanasiou, 2012). The addition of exogenous LINK protein to both aggrecan solutions (Tang, Buckwalter, & Rosenberg, 1996), isolated cells (Plaas, Sandy, & Kimura, 1988), and cell-seeded hydrogel constructs (Han et al., 2010) has shown that aggrecan retention through LINK-mediated stabilization is associated with increased compressive modulus. Similarly, the addition of the exogenous collagen crosslinking enzyme lysyl oxidase-like protein-2 (LOXL2) produces stable pyridinoline (PYR) crosslinks and enhances tensile strength (Makris,

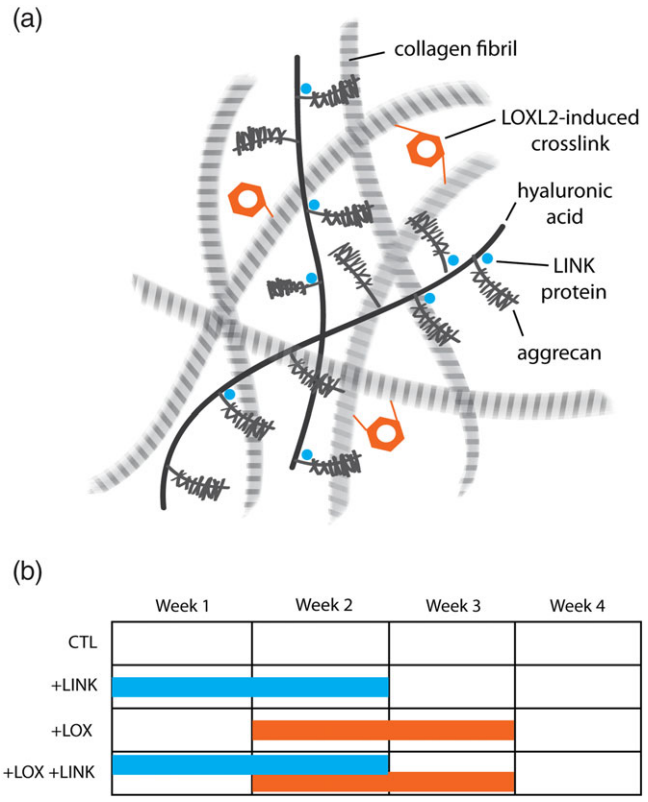

FIGURE 1 Schematic overview of the study. (a) Articular cartilage extracellular matrix. Exogenous addition of LOXL2 protein induces collagen crosslinking, whereas exogenous LINK protein binds aggrecan to the hyaluronic acid backbone of the proteoglycan aggregate. (b) Timing and duration of exogenous proteins in each treatment group. +LINK treatment occurred during Weeks 0–2, and +LOX treatment occurred during Weeks 1–3 [Colour figure can be viewed at wileyonlinelibrary.com]

MacBarb, Responte, Hu, & Athanasiou, 2013). The success of tissue-engineered articular cartilage replacement products *in vivo* depends heavily on the development of sufficient tensile and compressive properties (Huey, Hu, & Athanasiou, 2012; Makris, Gomoll, Malizos, Hu, & Athanasiou, 2015; Responte, Natoli, & Athanasiou, 2007). The development of quantitative, validated tools optimized specifically for monitoring the biochemical and mechanical properties of tissue-engineered articular cartilage is essential for evaluating these and other methods of improving tissue functionality (Morgan, Rose, & Matcher, 2014).

The ideal system for monitoring tissue maturation and development would allow repeated sterile measurements of developing tissue and incorporate some degree of automation to both sample assessment and data processing to determine whether release criteria are met prior to clinical use. A support vector machine (SVM) is a supervised machine learning technique that is widely used for classification of data into separate groups. The SVM algorithm uses a series of past observations or training data to learn how to automatically make accurate classification predictions about new, unknown data. The SVM divides separate experimental groups by constructing a multidimensional hyperplane decision boundary that maximizes the gap between the two group's data clusters. The SVM algorithm achieves high discriminative power between the groups by using nonlinear functions called kernels to transform the input space into a multidimensional space (Yu, Liu, Valdez, Gwinn, & Khoury, 2010). Previous studies have shown that SVM analysis can predict the proteoglycan content of tissue-engineered cartilage (Irrechukwu et al., 2012; Lin et al., 2012). Further efforts are needed to determine the predictive capabilities of SVM algorithms in identifying collagen crosslinking content in tissue-engineered articular cartilage.

The overall goal of this work is to study whether non-destructive optical methods have the potential to replace the conventional destructive measurements of tissue-engineered articular cartilage properties in an effort to reduce costs and research time and to allow for time-lapse measurements that track the maturation of individual samples. The objectives of this study were to (a) determine whether matrix stabilization though the addition of exogenous LOXL2 and LINK proteins would result in increased compressive and tensile properties in self-assembled articular cartilage constructs, (b) evaluate whether label-free, non-destructive FLIm could be used to infer the changes in both biochemical composition and biomechanical properties of tissue-engineered cartilage, (c) form specific, quantitative relationships between destructive and non-destructive measurements to determine whether the strength of these correlations are sufficient to replace destructive testing methods, and (d) determine whether SVM learning can predict LOXL2-induced collagen crosslinking in tissue-engineered articular cartilage. We hypothesized that FLIm could infer increases in both biochemical composition and biomechanical properties of self-assembled articular cartilage created through matrix stabilization with LOXL2 and LINK proteins and that a SVM built on FLIm-based parameters could identify collagen crosslinking.

2 | MATERIALS AND METHODS

2.1 | Chondrocyte isolation

Articular cartilage was harvested from the femoral condyles of five juvenile bovine stifle joints (Research 87, Boston, MA), minced, and digested in Dulbecco's Modified Eagle Medium (DMEM) with high glucose/GlutaMAX™-I (Life Technologies, Grand Island, NY) with 5% fetal bovine serum (HyClone, GE Healthcare Life Sciences, Marlborough, MA), 0.3% collagenase type II (Worthington, Lakewood, NJ), and 1% penicillin/streptomycin/fungizone (Lonza, Basel, Switzerland) for 18 hr on an orbital shaker at 37°C. Following digestion, the cells were filtered through 70-μm cell strainers and washed three times with DMEM. All donor cells were pooled prior to construct formation.

2.2 | Self-assembled construct culture

Constructs were formed using the self-assembling process, as previously described (Hu & Athanasiou, 2006). Briefly, 4×10^6 chondrocytes were suspended in 100 μl of a chondrogenic control (CTL) medium (Kwon et al., 2017) consisting of DMEM with 1% ITS+ premix (BD Biosciences, Bedford, MA), 1% non-essential amino acids (Life Technologies), 50 μg/ml of ascorbate-2-phosphate (Sigma-Aldrich, St. Louis, MO), 40 μg/ml of L-proline (Sigma-Aldrich), 100 μg/ml of sodium pyruvate (Sigma-Aldrich), 100 nM of dexamethasone (Sigma-Aldrich), and 1% penicillin/streptomycin/fungizone. Cell suspensions were seeded in nonadherent wells (5-mm diameter, 2% agarose) in 24-well plates (Costar, Corning, NY). After 4 hr, 400 μl of CTL medium was added to each well. Self-assembled constructs were cultured for 4 weeks in CTL medium only, CTL with 0.2 μg/ml of recombinant human LINK (R&D systems, Minneapolis, MN) added for Weeks 0–2 (+LINK), CTL with 0.146 μg/ml of hydroxylysine (Sigma-Aldrich), 0.0016 mg/ml of copper sulfate (Sigma-Aldrich), and 0.15 μg/ml of LOXL2 (SignalChem, Richmond, British Columbia, Canada) added for Weeks 1–3 (+LOX), or a combination of both exogenous factors (+LOX + LINK; Figure 1b). Constructs were removed from wells at Day 5, and 1 ml of fresh media was exchanged daily.

2.3 | Non-destructive optical assessment of self-assembled articular cartilage

At Week 4 in culture, a fiber-based, label-free fluorescence-based imaging system was used to make a non-destructive assessment of each cartilage construct (n = 6 per condition), followed by dissection for biochemical assays, mechanical evaluation, and histological processing (Figure 2a). The underlying principle of operation of the FLIm system has been previously reported (Y. Sun et al., 2009; Yankelevich et al., 2014). Time-resolved fluorescence was acquired by both systems using the pulse sampling technique (Marcu et al., 2014), and the decays were parameterized in postprocessing using a constrained

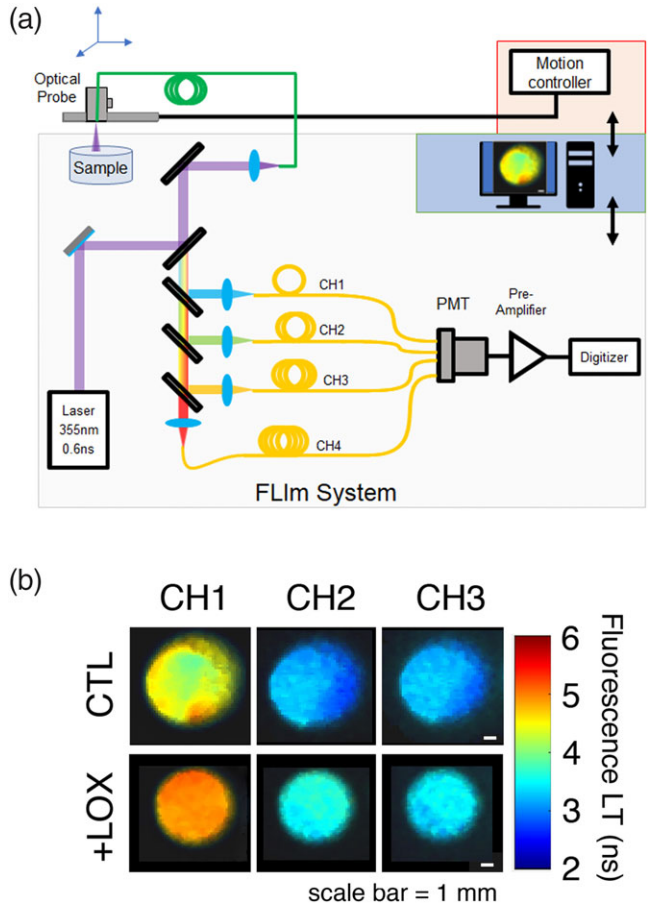

FIGURE 2 Optical system for assessing articular cartilage extracellular matrix. (a) Schematic of the FLImTRFS apparatus. A two-axis translation stage was used to scan a fiber optic across the sample. The fiber guides light from the laser and guides backscattered tissue autofluorescence to a custom-built wavelength selection module that separates the light into four spectral channels (CH1 = 375–410 nm, CH2 = 450–485 nm, CH3 = 515–565 nm, and CH4 = 595–660 nm). Complete mapping of a 6-mm-diameter sample occurs in under 10 min at a resolution of 20 μm per pixel. (b) Representative fluorescence lifetime imaging (FLIm) images of self-assembled constructs in the CH1, CH2, and CH3 spectral bands show increased lifetime (LT) with +LOX treatment over control (CTL) in all channels [Colour figure can be viewed at wileyonlinelibrary.com]

least squares deconvolution with Laguerre expansion (Liu et al., 2012). Average fluorescence LTs were calculated using the definition of intensity-weighted average LT (Yankelevich et al., 2014). A microchip laser (STV-02E-1 × 0, TEEM photonics, Grenoble, France) emitted optical pulses at a wavelength of 355 nm to generate sample autofluorescence. Light was delivered to and collected from the sample using a 2-m-long, flexible fiber optic cable (Molex, Lisle, IL) with an outer diameter of 480 μm. For optical assessment, the central 5-mm diameter cylindrical core (0.7–1.7 mm thick; Figure S3) from each sample was placed in a custom, glass sample holder in a Phosphate Buffered Saline (PBS) bath at room temperature. During imaging, the distal tip of the fiber was positioned approximately 1 mm above and perpendicular to the neocartilage surface. A two-axis digital translation stage (MX80L, Parker, Cleveland, OH) was used to scan the fiber across the sample surface. Samples were returned to 37°C immediately following imaging. The attenuation of 355-nm light in cartilage limits the penetration depth of FLIm to ~300 μm below the sample surface (Descalle, Jacques, Prahl, Laing, & Martin, 1998).

For FLIm, the fluorescence emission was separated into four spectral bands (CH1 = 375–410 nm, CH2 = 450–485 nm, CH3 = 515–565 nm, and CH4 = 595–660 nm) using a custom-built wavelength selection module. Each spectral band had an associated fiber optic delay line of different lengths (longer wavelength bands have longer delay lines). This arrangement allowed the four spectral bands to be temporally multiplexed onto a single photomultiplier tube (R5916U-50, Hamamatsu, Bridgewater, NJ), the voltage from which was digitized using a high-speed data acquisition board (PXIe-5185, National Instruments, Austin, TX) operating with a temporal resolution of 80 ps. This enabled complete mapping of the surface of the sample in approximately 10 min at a resolution of 200 μm per pixel. The mean and standard deviation of fluorescence LT in each spectral band were extracted from the FLIm images (Figure 2b) by defining circular regions of interest, centred on the sample that encompassed >75% of the surface area.

2.4 | Biochemical analysis and histology

For biochemical analysis, tissue samples were measured to obtain wet weight (ww) and dry weight (dw). Lyophilized samples were digested in papain for 18 hr at 60°C, as previously described (Kochiadakis et al., 2001). Sulfated GAG content was assayed using the Blyscan Glycosaminoglycan Assay kit (Biocolor, Westbury, NY). Total collagen content was quantified using a hydroxyproline assay (Biocolor; Woessner, 1961). PYR collagen crosslinks were analysed and quantified by high-performance liquid chromatography, as previously described (Bank et al., 1997). Constructs were acid digested and suspended in a solution of 0.5% heptafluorobutyric acid in 10% acetonitrile. Samples were injected into a Luna C18 column (Phenomenex, Torrance, CA) and eluted on a high-performance liquid chromatography system (Prominence UFLC, Shimadzu, Columbia, MD). A linear calibration curve was created using PYR standards (Quidel, San Diego, CA) for crosslink quantification. Collagen crosslinking density was defined as the molar ratio of PYR per collagen molecule and calculated assuming the molecular weight of the collagen triple helix of 300,000 MW (Haus, Carrithers, Trappe, & Trappe, 2007).

For histological evaluation, samples were fixed in 10% neutral buffered formalin, paraffin embedded, and then sectioned at 10 μm. Sections were stained with haematoxylin and eosin for general morphology, safranin O and nuclear fast green for glycosaminoglycans, or picrosirius red and nuclear fast green for total collagen following routine procedures. Picrosirius red stained collagen was visualized under polarized light microscopy to enhance natural birefringence (Junqueira, Bignolas, & Brentani, 1979; Puchtler, Waldrop, & Valentine, 1973).

2.5 | Compressive and tensile testing

Compressive properties were quantified by coring a 2-mm cylindrical punch from each construct, as previously described (Allen & Athanasiou, 2006). Briefly, compression testing is accomplished in two phases: height detection and stress relaxation testing in unconfined compression. Samples were equilibrated in a PBS bath, loaded to 0.02 N load to determine sample thickness and preconditioned under 15 cycles of 5% strain. Samples were loaded under 10% strain for 600 s immediately followed by 20% strain for 900 s to obtain equilibrium (Figure S1). Force-displacement data were recorded, converted to stress–strain based on sample dimensions, and all data were analysed using biphasic theory (Mak, Lai, & Mow, 1987) in Matlab (Mathworks, Natick, MA) to calculate instantaneous modulus, relaxation modulus, and coefficient of viscosity for each sample.

Tensile testing was conducted using a uniaxial materials testing machine (Test Resources, Shakopee, MN), as previously described (Makris et al., 2013). Briefly, cartilage samples were cut into dog bone-shaped tensile specimens, and the sample thickness and width were measured via ImageJ software (NIH, Bethesda, MD; Schindelin, Rueden, Hiner, & Eliceiri, 2015). A uniaxial strain to failure test was conducted with a fixed gauge length of 1.3 mm and a strain rate of 1% of the gauge length per second. Load–displacement curves were normalized to specimen cross-sectional area, and the apparent Young's modulus was calculated by least squares fitting the linear portion of the resulting stress–strain curve in Matlab (Mathworks). Ultimate tensile strength (UTS) was defined at the maximum stress.

2.6 | Statistical analysis and modelling

All evaluations in this study were performed using $n = 6$ matched samples per treatment group on JMP v13 (SAS Institute, Cary, NC). Statistical analysis of groups was performed using one-way analysis of variance with Tukey's post hoc analysis. Bar chart data are presented as mean ± standard deviation with significant differences ($p < 0.05$) indicated by bars not sharing the same letter. Bars with the same letter are not significantly different from one another, and bars with more than one letter reflect overlap between groups. Correlations between bivariate parameters of each treatment were modelled separately to determine which outcome parameter correlated with which biochemical component using simple linear least squares regression analysis.

2.7 | SVM development

SVM algorithms with a (Gaussian) radial basis function kernel (Chang & Lin, 2011; H. W. Wang, Lin, Pai, & Chang, 2011) were tested for their ability to predict LOXL2-induced collagen crosslinking in self-assembled constructs. The feature vector included average fluorescence LT and intensity values from CH1, CH2, and CH3. Due to the range of FLIm signal across the engineered tissue samples, we defined the accuracy of the classification as the ratio of correctly classified pixels to the total number of pixels in the image. Artifacts due to low signal to noise ratio and edge effects were removed by data thresholding. A receiver operating characteristic curve was generated to evaluate the quality of a binary classification test and to graphically illustrate the diagnostic ability of the SVM classifier as the discriminant threshold was varied. Sensitivity, specificity, and positive predictive values were calculated using a leave-one-out cross-validation approach (Hsu & Lin, 2002). This involved sequentially leaving data from a single specimen out of the training set and then testing the classification accuracy on that single specimen for all specimens. Data processing, image analysis, and classification were performed using MATLAB (Mathworks).

3 | RESULTS

3.1 | Exogenous LOXL2 and LINK proteins enhanced extracellular matrix stabilization in self-assembled constructs

The self-assembling process resulted in flat, uniform neocartilage formation in all culture conditions tested (Figure 3a). Matrix stabilization with LOXL2 and LINK proteins resulted in increased collagen birefringence and proteoglycan (Gago et al., 2009) staining as compared with CTL (Figure 3b). Proteoglycan content was significantly increased with both +LOX and +LOX + LINK treatments (1.5- and 1.4-fold respectively, $p < 0.001$; Figure 4a). Treatment did not significantly alter collagen content ($p = 0.43$; 4.64 ± 0.57% COL/dw for all groups), but both +LOX and +LOX + LINK treatments produced large increases in collagen crosslinking density (2.9- and 4.9-fold respectively, $p < 0.0001$; Figure 4b).

3.2 | Matrix stabilization improved both tensile and compressive mechanical properties

The relaxation modulus was significantly increased with both +LOX and +LOX + LINK treatments as compared with CTL (5.9- and 3.4-fold, respectively, $p < 0.001$; Figure 4c). Similarly, the instantaneous modulus was significantly increased with both +LOX and +LOX + LINK treatments as compared with CTL (3.9- and 2.1-fold respectively, $p < 0.001$; Figure 4d). The coefficient of viscosity was significantly increased with +LOX treatment as compared with CTL (7.2-fold, $p < 0.0001$; Figure S2B). Compared with CTL, tensile Young's modulus significantly increased 2.0-fold with +LOX and 3.8-fold with +LOX + LINK treatment to reach an average value of 1.98 ± 0.68 MPa ($p < 0.01$; Figure 4e). UTS was also significantly increased with both +LOX and +LOX + LINK treatments as compared with CTL (6.2- and 8.3-fold, respectively, $p = 0.001$; Figure 4f).

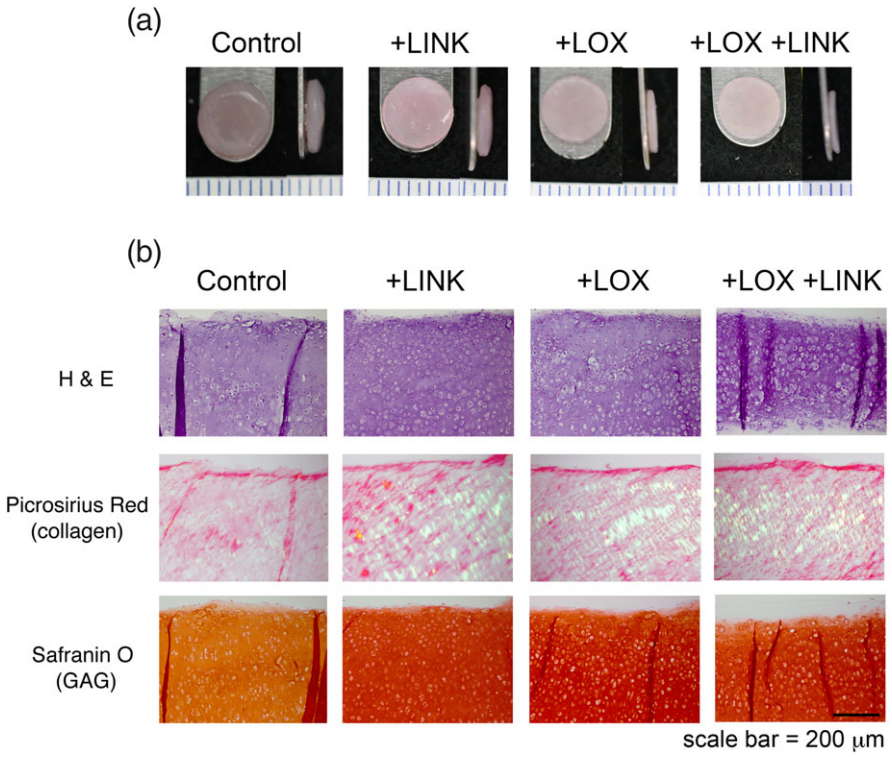

FIGURE 3 Enhanced extracellular matrix in self-assembled constructs with the addition of exogenous LOXL2 and LINK proteins. (a) At 4 weeks, all groups produced uniform, flat constructs. Ruler = 1 mm. (b) Histological staining showed increased picrosirius red birefringence and safranin O staining in +LINK, +LOX, and +LOX + LINK groups over control. Scale bar = 200 μm [Colour figure can be viewed at wileyonlinelibrary.com]

3.3 | Destructive and non-destructive testing detect changes in matrix stabilization and mechanical properties

FLIm CH1 and CH3 LT were significantly increased with the addition of exogenous proteins ($p < 0.001$ and $p = 0.02$, respectively; Figure 4g,h). Destructive biochemical assays had strong significant correlations with both tensile and compressive mechanical properties. Proteoglycan content (GAG/ww) had a strong and significant correlation with compressive modulus ($R^2 = 0.68$; $p < 0.001$; Figure 5a). UTS had a strong and significant correlation with collagen crosslinking density (PYR/COL; $R^2 = 0.63$; $p < 0.001$; Figure 5b). Non-destructive fluorescence LT was able to detect changes in biochemical content. FLIm CH3 LT had moderate significant correlation with GAG/ww ($R^2 = 0.49$; $p = 0.001$; Figure 5c), and FLIm CH1 LT has a significant correlation with PYR/COL ($R^2 = 0.45$; $p = 0.002$; Figure 5d). Non-destructive fluorescence LT was able to detect changes in both tensile and compressive mechanical properties. FLIm CH3 LT had a strong and significant correlation with compressive modulus ($R^2 = 0.59$; $p < 0.001$; Figure 5e). FLIm CH1 LT had a strong and significant correlation with the UTS ($R^2 = 0.82$; $p < 0.0001$; Figure 5f) and a moderate significant correlation with the coefficient of viscosity ($R^2 = 0.50$; $p < 0.002$; Figure S2B).

3.4 | SVM learning identifies LOXL2-induced collagen crosslinking in tissue-engineered neocartilage

SVM classification was able to identify LOXL2-induced collagen crosslinking in the self-assembled neocartilage using fluorescence-based parameters. Fluorescence LT in all three spectral channels increased with +LOX treatment as compared with CTL and allowed +LOX detection as observed from parameter distributions (Figure 6 a). An SVM was built using the three fluorescence-based parameters CH1 intensity ratio, CH1 LT, and CH2 LT. The three-dimensional scatter plot of training data shows the SVM classifier hyperplane as a decision boundary for +LOX classification (Figure 6b). The area under the curve was used to determine the discriminant ability of the SVM classifier as 98.4% (Figure 6c). The diagnostic ability of the SVM was dependent on the number of pixels analysed in the region of interest with higher pixel numbers improving the discriminant ability of the classification. Increasing pixel number from 100 to 500 pixels improved sensitivity (true positive rate) from 0.94 to 0.98 and improved specificity (1-false positive rate) from 0.75 to 0.88 (Figure 6d).

4 | DISCUSSION

The novel findings of this study include (a) enhanced tensile and compressive properties (8.3- and 5.9-fold, respectively) through matrix stabilization with a combination of LOXL2 and LINK proteins, (b) quantitative relationships between FLIm CH3 LT signal and compressive relaxation modulus ($R^2 = 0.59$; $p < 0.001$), (c) quantitative relationships between FLIm CH1 LT signal and tensile strength ($R^2 = 0.82$; $p < 0.001$), and (d) automated SVM classification of collagen crosslinking in self-assembled neocartilage using fluorescence-based parameters (discriminant ability of 98.4%).

Biochemical properties of self-assembled articular cartilage were enhanced through matrix stabilization with exogenous LOXL2 and

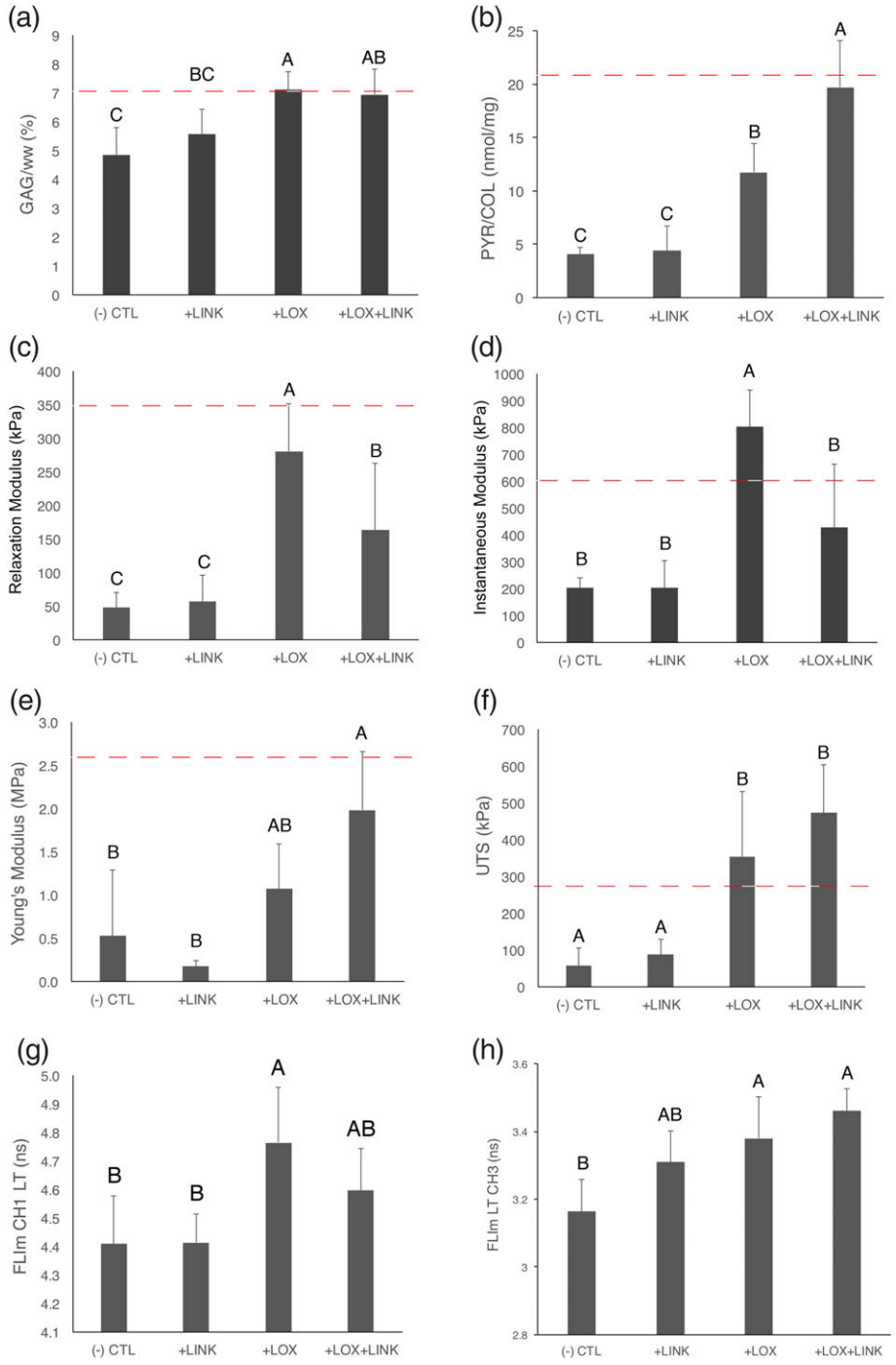

FIGURE 4 Matrix stabilization increased biochemical, mechanical, and optical properties of self-assembled neocartilage. (a) Proteoglycan content was increased in both +LOX and +LOX + LINK treatments over control (CTL). (b) Collagen crosslinking density was significantly increased with the combined +LOX + LINK treatment over +LOX alone. Both +LOX and +LOX + LINK treatments increased compressive relaxation modulus (c) and ultimate tensile strength (f) over CTL. Instantaneous modulus was increased with +LOX (d) and tensile Young's modulus was increased with +LOX + LINK treatment over CTL. Non-destructive optical parameter FLIm CH1 LT was significantly increased with +LOX treatment (g) and FLIm CH3 LT was significantly increased with +LOX and + LOX + LINK (h) over CTL. Red dashed lines represent native values (Paschos, Lim, Hu, & Athanasiou, 2017) [Colour figure can be viewed at wileyonlinelibrary.com]

LINK proteins. Increases in proteoglycan content were seen with the addition of LOXL2 and LINK proteins in quantitative assays (1.5- and 1.4-fold, respectively) and qualitatively with increased safranin O staining. Although the total collagen content was not significantly altered, matrix stabilization with LOXL2 and LINK proteins resulted in a more aligned collagen fiber orientation as observed in increased collagen birefringence in histological sections. In addition to increased structural alignment, treatment with LOXL2 and LINK increased total crosslinking density in neocartilage by 4.6-fold as compared with CTL. Because collagen architecture and strength are critical to

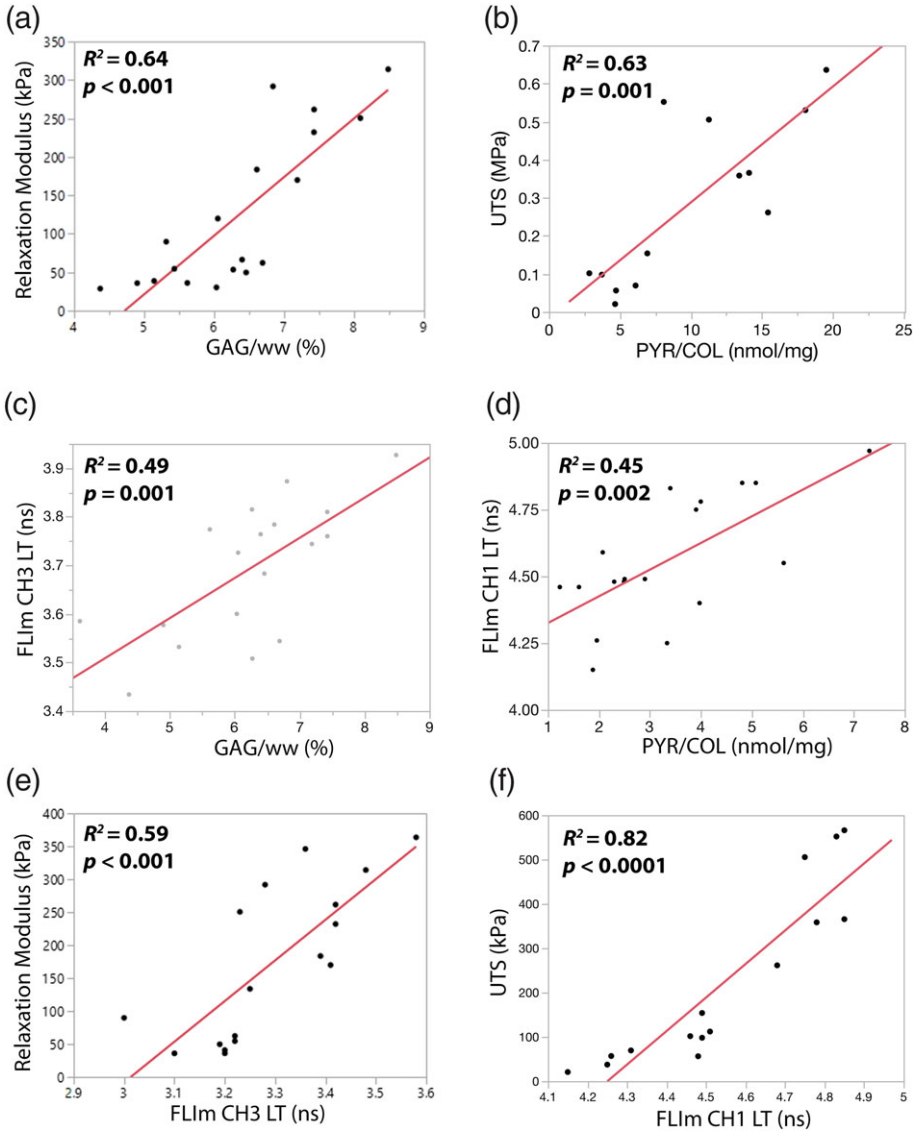

FIGURE 5 Destructive and non-destructive tests detect changes in matrix stabilization and mechanical properties. Destructive biochemical assays showed strong correlations between (a) compressive relaxation modulus and proteoglycan content (GAG/ww) and (b) ultimate tensile strength and collagen crosslinking density (PYR/COL). Non-destructive optical assays showed significant correlations between (c) FLIm CH3 LT and GAG/ww, (d) FLIm CH1 LT and PYR/COL, (e) compressive modulus and FLIm CH3 LT, and (f) ultimate tensile strength and FLIm CH1 LT [Colour figure can be viewed at wileyonlinelibrary.com]

cartilage function and durability, the exogenous addition of matrix stabilizing proteins like LOXL2 and LINK may be warranted to ensure the long-term success of repair cartilage.

During loading, the collagen network helps resist lateral expansion of the cartilage and creates a mesh-like structure that traps the large, hydrophilic proteoglycan aggregates and allows for osmotic pressure build-up and tissue load-bearing capabilities (Park, Krishnan, Nicoll, & Ateshian, 2003). This interplay is dependent on the intrinsic stiffness and strength of each of the matrix components. For cartilage, they depend upon the tensile properties of collagen fibrils and the compressive stiffness of proteoglycan aggregates, as well as the strength of the interfacial bonds among these components. The combination of increased collagen fiber alignment and collagen crosslinking density directly translated into increases in tensile Young modulus (3.8-fold over CTL) and UTS (8.3-fold over CTL). LINK protein has been shown to bind to the bone morphogenetic protein receptor-II on chondrocytes, initiating an increased expression of the chondrocyte-specific transcription factor SOX 9 and collagen type-II (Z. Wang et al., 2013). Through such binding activities, LINK protein may be involved in regulating the content, formation, and the morphology of collagen fibrils. The synergistic increase in collagen crosslinking density with the combination of +LOX + LINK treatment (4.6-fold over CTL) as compared with +LOX treatment alone (2.4-fold over CTL) may be partially attributed to the ability of LINK protein to directly regulate cellular biochemical processes in addition to LOX having a known effect on collagen crosslinking. LINK protein has been shown to directly bind fibrillar collagen and increase collagen fiber diameter (Chandrasekhar et al., 1984) and to bind epidermal growth factor

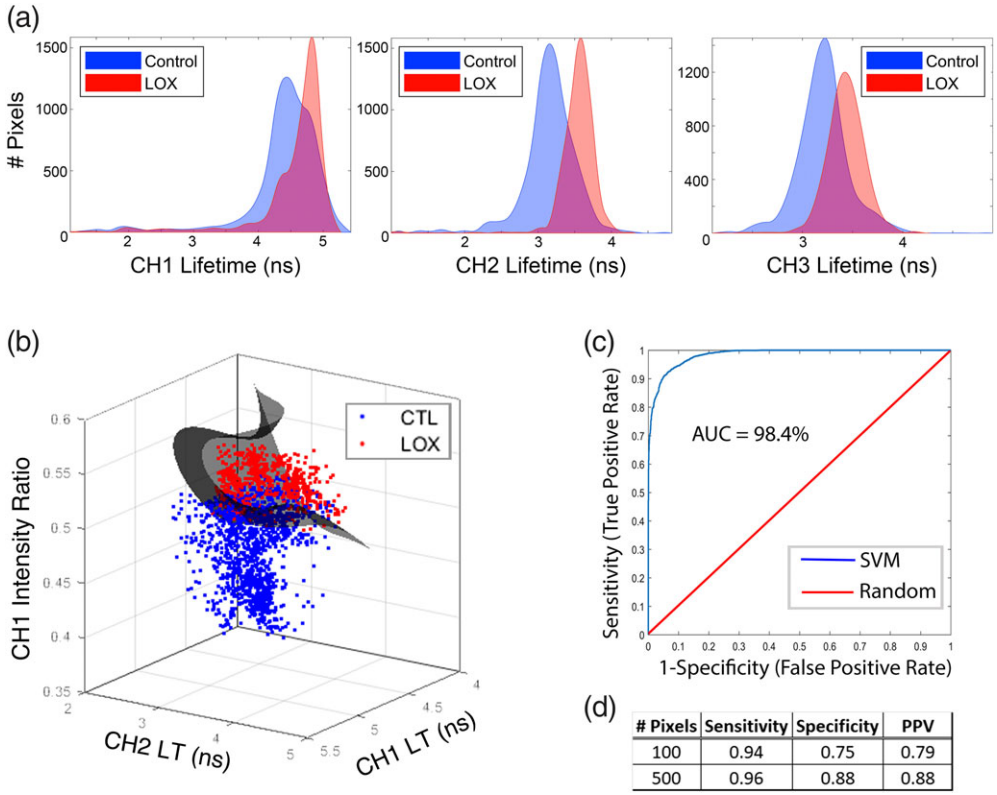

# Pixels	Sensitivity	Specificity	PPV
100	0.94	0.75	0.79
500	0.96	0.88	0.88

FIGURE 6 Support vector machine (SVM) learning identifies LOXL2-induced collagen crosslinking in tissue-engineered neocartilage. (a) Fluorescence lifetime (LT) distributions for control and LOXL2-treated neocartilage in spectral channels CH1, CH2, and CH3 show increased LT with +LOX treatment compared with control. (b) Three-dimensional scatter plot of training data for +LOX detection. The SVM classifier hyperplane (grey) acts as a decision boundary for classification. (c) Diagnostic ability of the classifier system. A receiver operating characteristic curve graphically illustrates the diagnostic ability of the SVM classifier as the discriminant threshold is varied. The discriminant ability of the SVM classifier according to the area under the curve is 98.4%. (d) Summary table shoes strong performance values of the support vector machine algorithm for +LOX classification with sensitivity, specificity, and positive predictive value (PPV). Performance increased with increased number of pixels evaluated per sample [Colour figure can be viewed at wileyonlinelibrary.com]

receptors (Spicer, Joo, & Bowling, 2003) resulting in increased cartilage mechanical strength (Jia et al., 2016).

Matrix stabilization improved the compressive properties of the self-assembled neocartilage. Large increases in compressive modulus (3.9-fold over CTL) were observed with a combination of LOXL2 and LINK proteins. The increases in compressive properties with the addition of exogenous proteins may be partially attributed to the role that aggrecan aggregate size plays in determining cartilage mechanical strength. Although LINK protein was not found to increase the total GAG content, it has been shown to increase aggrecan aggregate size by providing an almost irreversible tertiary bond between aggrecan and the core protein hyaluronan (Kiani et al., 2002). Increases in aggregate size have been shown to increase the average strength of the proteoglycan network and, ultimately, the tissue itself (Zhu, Lai, & Mow, 1991). In this way, the stabilization of aggregates by LINK protein may play a significant role in maintaining the organization and attachment of the collagen fiber-reinforced proteoglycan matrix and its intrinsic mechanical properties.

Neocartilage constructs with +LOX and +LINK treatments had tensile properties on par with those of native, juvenile femoral cartilage, and the compressive relaxation modulus reached 86% of native values (300 kPa compared with 350 kPa for the native tissue; Paschos et al., 2017). The lower proteoglycan content at 4 weeks in culture (~7% in neocartilage as compared with ~14% in native tissue; Paschos et al., 2017) may partially account for lower compressive stiffness. Self-assembled neocartilage has been shown to increase in proteoglycan content and compressive properties over longer in vitro (Ofek et al., 2008) and *in vivo* (Responte, Arzi, Natoli, Hu, & Athanasiou, 2012) culture periods suggesting the possibility that full biomechanical functionality is achievable.

The non-destructive FLIm techniques detected changes in collagen crosslinking density, proteoglycan content, and changes in the tensile and compressive properties of tissue-engineered cartilage that occur with matrix stabilization. The strong linear correlations between destructive and non-destructive tests (R^2 = 0.82 and R^2 = 0.59 for FLIm vs. tensile and compressive properties, respectively) support the hypothesis that non-destructive assessments could be used to infer the differences in the mechanical properties of self-assembled cartilage. We specified that spectral bands at 375–410 nm (CH1) and 515–565 nm (CH3) are important for the assessment of the tensile and compressive properties of tissue-engineered cartilage, a finding that will be of high interest for the fields of cell biology and

regenerative medicine. The lack of depth-dependent variations in the biochemical composition in the neocartilage reduced bias created by comparing FLIm surface measurements (~300 μm) with full thickness biochemical and mechanical properties. In contrast, native cartilage has a large depth-dependent variation in biochemical composition. When we subjected native tissue to enzymatic treatments to deplete matrix content, we found lower than expected differences in fluorescence signal in cartilage imaged perpendicular to the tissue surface as compared with cartilage imaged in cross section (Zhou et al., 2018).

SVM learning classification was able to identify LOXL2-induced collagen crosslinking in the self-assembled neocartilage using fluorescence-based parameters. Distinct fluorescence LT distributions for CTL and LOXL2 cross-linked samples allowed the SVM classifier to distinguish between groups with a discriminant ability of 98.4%. Our work provides a promising proof of principle by demonstrating the predictive power of the SVM to detect differences in collagen crosslinking content with just a small set of variables. This classification approach can be extended to include larger data sets and incorporate other variables, such as proteoglycan content, to generate an automated system to assess cartilage tissue maturation and determine whether release criteria are met prior to clinical use.

A major challenge in the research and translation of tissue-engineered products is the cost and time associated with destructive testing methods. The inexpensive, fiber-based interface of the FLIm-based system can be incorporated into a standard biosafety cabinet for sterile imaging and repeated measurements of samples (Sherlock, et al., 2018). The ability to continuously monitor tissue quality enables quick adjustments to varying rates of tissue development, the scrapping and restarting of poorly developing tissue, and predictive capabilities of final tissue quality.

4.1 | Conclusions

Matrix stabilization using a combination of exogenous LOXL2 and LINK proteins produces robust self-assembled cartilage with increased tensile and compressive properties on par with native tissue. Fluorescence LT is capable of detecting the biological and mechanical changes that occur with matrix stabilization. These data, combined with fiber optic-based instrumentation, suggest that FLIm-based tools are a potential non-destructive method for quantitatively monitoring the growth and quality of tissue-engineered articular cartilage. The use of continuous monitoring strategies could represent a significant element in reducing costs in research, meeting the FDA regulatory requirements for compliant manufacturing in industry, and as a diagnostic tool in the clinic. The methods presented here can be adapted to other tissue engineering and regenerative medicine applications.

ACKNOWLEDGEMENTS

This work was funded by the California Institute for Regenerative Medicine (CIRM) Grant RT3-07981 and the National Institutes of Health (NIH) Grant R01AR067821.

CONFLICT OF INTEREST

The authors have declared that there is no conflict of interest.

ORCID

Anne K. Haudenschild https://orcid.org/0000-0003-0520-4224
Kyriacos A. Athanasiou https://orcid.org/0000-0001-5387-8405

REFERENCES

Alfonso-Garcia, A., Haudenschild, A. K., & Marcu, L. (2018). Label-free assessment of carotid artery biochemical composition using fiber-based fluorescence lifetime imaging. *Biomedical Optics Express*, *9*(9), 4064–4076. https://doi.org/10.1364/BOE.9.004064

Allen, K. D., & Athanasiou, K. A. (2006). Viscoelastic characterization of the porcine temporomandibular joint disc under unconfined compression. *Journal of Biomechanics*, *39*(2), 312–322. https://doi.org/10.1016/j.jbiomech.2004.11.012

Angheloiu, G. O., Haka, A. S., Georgakoudi, I., Arendt, J., Müller, M. G., Scepanovic, O. R., … Feld, M. S. (2011). Detection of coronary atherosclerotic plaques with superficial proteoglycans and foam cells using real-time intrinsic fluorescence spectroscopy. *Atherosclerosis*, *215*(1), 96–102. https://doi.org/10.1016/j.atherosclerosis.2010.11.020

Bank, R. A., Beekman, B., Verzijl, N., de Roos, J. A. D. M., Sakkee, A. N., & TeKoppele, J. M. (1997). Sensitive fluorimetric quantitation of pyridinium and pentosidine crosslinks in biological samples in a single high-performance liquid chromatographic run. *Journal of Chromatography B, Biomedical Sciences and Applications*, *703*(1–2), 37–44. https://doi.org/10.1016/S0378-4347(97)00391-5

Chandrasekhar, S., Kleinman, H. K., Hassell, J. R., Martin, G. R., Termine, J. D., & Trelstad, R. L. (1984). Regulation of type I collagen fibril assembly by link protein and proteoglycans. *Collagen and Related Research*, *4*(5), 323–337. https://doi.org/10.1016/S0174-173X(84)80001-1

Chang, C.-C., & Lin, C.-J. (2011). LIBSVM: A library for support vector machines. *ACM Transactions on Intelligent Systems and Technology (TIST)*, *2*(3), 27.

Descalle, M. A., Jacques, S. L., Prahl, T. J., Laing, T. J., & Martin, W. R. (1998). Measurements of ligament and cartilage optical properties at 351 nm, 365 nm and in the visible range (440–800 nm). *Laser-Tissue Interaction, Tissue Optics, and Laser Welding III, Proceedings of SPIE*, *3195*, 280–286.

FDA. 2011. Guidance for industry: Potency tests for cellular and gene therapy products. In: Services USDoHaH, editor.

Fite, B. Z., Decaris, M., Sun, Y., Sun, Y., Lam, A., Ho, C. K. L., … Marcu, L. (2011). Noninvasive multimodal evaluation of bioengineered cartilage constructs combining time-resolved fluorescence and ultrasound imaging. *Tissue Engineering. Part C, Methods*, *17*(4), 495–504. https://doi.org/10.1089/ten.tec.2010.0368

Gago, N., Perez-Lopez, V., Sanz-Jaka, J. P., Cormenzana, P., Eizaguirre, I., Bernad, A., & Izeta, A. (2009). Age-dependent depletion of human skin-derived progenitor cells. *Stem Cells*, *27*(5), 1164–1172. https://doi.org/10.1002/stem.27

Gorpas, D., Fatakdawala, H., Bec, J., Ma, D., Yankelevich, D. R., Qi, J., & Marcu, L. (2015). Fluorescence lifetime imaging and intravascular ultrasound: Co-registration study using ex vivo human coronaries. *IEEE Transactions on Medical Imaging*, *34*(1), 156–166. https://doi.org/10.1109/TMI.2014.2350491

Gorpas, D., Ma, D., Bec, J., Yankelevich, D. R., & Marcu, L. (2016). Real-time visualization of tissue surface biochemical features derived from fluorescence lifetime measurements. *IEEE Transactions on Medical*

Imaging, *35*(8), 1802–1811. https://doi.org/10.1109/TMI.2016.2530621

Han, E. H., Wilensky, L. M., Schumacher, B. L., Chen, A. C., Masuda, K., & Sah, R. L. (2010). Tissue engineering by molecular disassembly and reassembly: Biomimetic retention of mechanically functional aggrecan in hydrogel. *Tissue Engineering. Part C, Methods*, *16*(6), 1471–1479. https://doi.org/10.1089/ten.tec.2009.0800

Hardingham, T. E. (1979). The role of link-protein in the structure of cartilage proteoglycan aggregates. *The Biochemical Journal*, *177*(1), 237–247. https://doi.org/10.1042/bj1770237

Haudenschild, A. K., Sherlock, B. E., Zhou, X., Hu, J. C., Leach, J. K., Marcu, L., & Athanasiou, K. A. (2018). Nondestructive fluorescence lifetime imaging and time-resolved fluorescence spectroscopy detect cartilage matrix depletion and correlate with mechanical properties. *European Cells & Materials*, *36*, 30–43. https://doi.org/10.22203/eCM.v036a03

Haus, J. M., Carrithers, J. A., Trappe, S. W., & Trappe, T. A. (2007). Collagen, cross-linking, and advanced glycation end products in aging human skeletal muscle. *Journal of applied physiology (Bethesda, MD: 1985)*, *103*(6), 2068–2076. https://doi.org/10.1152/japplphysiol.00670.2007

Hsu, C.-W., & Lin, C.-J. (2002). A comparison of methods for multiclass support vector machines. *IEEE Transactions on Neural Networks*, *13*(2), 415–425. https://doi.org/10.1109/72.991427

Hu, J. C., & Athanasiou, K. A. (2006). A self-assembling process in articular cartilage tissue engineering. *Tissue Engineering*, *12*(4), 969–979. https://doi.org/10.1089/ten.2006.12.969

Huey, D. J., Hu, J. C., & Athanasiou, K. A. (2012). Unlike bone, cartilage regeneration remains elusive. *Science*, *338*(6109), 917–921. https://doi.org/10.1126/science.1222454

Irrechukwu, O. N., Reiter, D. A., Lin, P. C., Roque, R. A., Fishbein, K. W., & Spencer, R. G. (2012). Characterization of engineered cartilage constructs using multiexponential T(2) relaxation analysis and support vector regression. *Tissue Engineering. Part C, Methods*, *18*(6), 433–443. https://doi.org/10.1089/ten.tec.2011.0509

Jia, H., Ma, X., Tong, W., Doyran, B., Sun, Z., Wang, L., … Qin, L. (2016). EGFR signaling is critical for maintaining the superficial layer of articular cartilage and preventing osteoarthritis initiation. *Proceedings of the National Academy of Sciences of the United States of America*, *113*(50), 14360–14365. https://doi.org/10.1073/pnas.1608938113

Junqueira, L. C. U., Bignolas, G., & Brentani, R. R. (1979). Picrosirius staining plus polarization microscopy, a specific method for collagen detection in tissue sections. *The Histochemical Journal*, *11*(4), 447–455. https://doi.org/10.1007/BF01002772

Kiani, C., Chen, L., Wu, Y. J., Albert, J. Y., & Burton, B. Y. (2002). Structure and function of aggrecan. *Cell Research*, *12*, 19–32. https://doi.org/10.1038/sj.cr.7290106

Kochiadakis, G. E., Chrysostomakis, S. I., Kalebubas, M. D., Filippidis, G. M., Zacharakis, I. G., Papazoglou, T. G., & Vardas, P. E. (2001). The role of laser-induced fluorescence in myocardial tissue characterization: An experimental in vitro study. *Chest*, *120*(1), 233–239. https://doi.org/10.1378/chest.120.1.233

Kwon, H., Haudenschild, A. K., Brown, W. E., Vapniarsky, N., Paschos, N. K., Arzi, B., … Athanasiou, K. A. (2017). Tissue engineering potential of human dermis-isolated adult stem cells from multiple anatomical locations. *PLoS ONE*, *12*(8), e0182531. https://doi.org/10.1371/journal.pone.0182531

Lin, P. C., Irrechukwu, O., Roque, R., Hancock, B., Fishbein, K. W., & Spencer, R. G. (2012). Multivariate analysis of cartilage degradation using the support vector machine algorithm. *Magnetic Resonance in Medicine*, *67*(6), 1815–1826. https://doi.org/10.1002/mrm.23189

Liu, J., Sun, Y., Qi, J., & Marcu, L. (2012). A novel method for fast and robust estimation of fluorescence decay dynamics using constrained least-squares deconvolution with Laguerre expansion. *Physics in Medicine and Biology*, *57*(4), 843–865. https://doi.org/10.1088/0031-9155/57/4/843

Mak, A. F., Lai, W. M., & Mow, V. C. (1987). Biphasic indentation of articular cartilage—I. Theoretical analysis. *Journal of Biomechanics*, *20*(7), 703–714.

Makris, E. A., Gomoll, A. H., Malizos, K. N., Hu, J. C., & Athanasiou, K. A. (2015). Repair and tissue engineering techniques for articular cartilage. *Nature Reviews Rheumatology*, *11*(1), 21–34. https://doi.org/10.1038/nrrheum.2014.157

Makris, E. A., MacBarb, R. F., Responte, D. J., Hu, J. C., & Athanasiou, K. A. (2013). A copper sulfate and hydroxylysine treatment regimen for enhancing collagen cross-linking and biomechanical properties in engineered neocartilage. *The FASEB Journal*, *27*(6), 2421–2430. https://doi.org/10.1096/fj.12-224030

Manning, H. B., Nickdel, M. B., Yamamoto, K., Lagarto, J. L., Kelly, D. J., Talbot, C. B., … Itoh, Y. (2013). Detection of cartilage matrix degradation by autofluorescence lifetime. *Matrix Biology*, *32*(1), 32–38. https://doi.org/10.1016/j.matbio.2012.11.012

Marcu, L., French, P. M. W., & Elson, D. S. (2014). *Fluorescence lifetime spectroscopy and imaging: Principles and applications in biomedical diagnostics*. Boca Raton: CRC Press/Taylor & Francis Group. https://doi.org/10.1201/b17018

Morgan, S. P., Rose, F. R., & Matcher, S. J. (2014). *Optical techniques in regenerative medicine*. Boca Raton: Taylor & Francis.

Ofek, G., Revell, C. M., Hu, J. C., Allison, D. D., Grande-Allen, K. J., & Athanasiou, K. A. (2008). Matrix development in self-assembly of articular cartilage. *PLoS ONE*, *3*(7), e2795. https://doi.org/10.1371/journal.pone.0002795

Park, S., Krishnan, R., Nicoll, S. B., & Ateshian, G. A. (2003). Cartilage interstitial fluid load support in unconfined compression. *Journal of Biomechanics*, *36*(12), 1785–1796. https://doi.org/10.1016/S0021-9290(03)00231-8

Paschos, N. K., Lim, N., Hu, J. C., & Athanasiou, K. A. (2017). Functional properties of native and tissue-engineered cartilage toward understanding the pathogenesis of chondral lesions at the knee: A bovine cadaveric study. *Journal of Orthopaedic Research*, *35*(11), 2452–2464. https://doi.org/10.1002/jor.23558

Plaas, A. H., Sandy, J. D., & Kimura, J. H. (1988). Biosynthesis of cartilage proteoglycan and link protein by articular chondrocytes from immature and mature rabbits. *The Journal of Biological Chemistry*, *263*(16), 7560–7566.

Puchtler, H., Waldrop, F. S., & Valentine, L. S. (1973). Polarization microscopic studies of connective tissue stained with picro-sirius red FBA. *Beiträge Zur Pathologie*, *150*(2), 174–187. https://doi.org/10.1016/S0005-8165(73)80016-2

Responte, D. J., Arzi, B., Natoli, R. M., Hu, J. C., & Athanasiou, K. A. (2012). Mechanisms underlying the synergistic enhancement of self-assembled neocartilage treated with chondroitinase-ABC and TGF-beta1. *Biomaterials*, *33*(11), 3187–3194. https://doi.org/10.1016/j.biomaterials.2012.01.028

Responte, D. J., Natoli, R. M., & Athanasiou, K. A. (2007). Collagens of articular cartilage: Structure, function, and importance in tissue engineering. *Critical Reviews in Biomedical Engineering*, *35*(5), 363–411. https://doi.org/10.1615/CritRevBiomedEng.v35.i5.20

Schindelin, J., Rueden, C. T., Hiner, M. C., & Eliceiri, K. W. (2015). The ImageJ ecosystem: An open platform for biomedical image analysis. *Molecular Reproduction and Development*, *82*(7–8), 518–529. https://doi.org/10.1002/mrd.22489

Setton, L. A., Mow, V. C., Muller, F. J., Pita, J. C., & Howell, D. S. (1993). Altered structure-function relationships for articular cartilage in human

osteoarthritis and an experimental canine model. *Agents and Actions. Supplements*, *39*, 27–48.

Seyfried, N. T., McVey, G. F., Almond, A., Mahoney, D. J., Dudhia, J., & Day, A. J. (2005). Expression and purification of functionally active hyaluronan-binding domains from human cartilage link protein, aggrecan and versican: Formation of ternary complexes with defined hyaluronan oligosaccharides. *The Journal of Biological Chemistry*, *280*(7), 5435–5448. https://doi.org/10.1074/jbc.M411297200

Sherlock, B. E., Harvestine, J. N., Mitra, D., Haudenschild, A., Hu, J., Athanasiou, K. A., (2018) Nondestructive assessment of collagen hydrogel cross-linking using time-resolved autofluorescence imaging. *J Biomed Opt*, *23*(3):1–9

Spicer, A. P., Joo, A., & Bowling, R. A. (2003). A hyaluronan binding link protein gene family whose members are physically linked adjacent to chrondroitin sulfate proteoglycan core protein genes: THE MISSING LINKS. *Journal of Biological Chemistry*, *278*(23), 21083–21091. https://doi.org/10.1074/jbc.M213100200

Sun, M. Y., Yoo, E., Green, B. J., Altamentova, S. M., Kilkenny, D. M., & Rocheleau, J. V. (2012). Autofluorescence imaging of living pancreatic islets reveals fibroblast growth factor-21 (FGF21)-induced metabolism. *Biophysical Journal*, *103*(11), 2379–2388. https://doi.org/10.1016/j.bpj.2012.10.028

Sun, Y., Park, J., Stephens, D. N., Jo, J. A., Sun, L., Cannata, J. M., … Marcu, L. (2009). Development of a dual-modal tissue diagnostic system combining time-resolved fluorescence spectroscopy and ultrasonic backscatter microscopy. *The Review of Scientific Instruments*, *80*(6), 065104. https://doi.org/10.1063/1.3142478

Tang, L. H., Buckwalter, J. A., & Rosenberg, L. C. (1996). Effect of link protein concentration on articular cartilage proteoglycan aggregation. *Journal of Orthopaedic Research*, *14*(2), 334–339. https://doi.org/10.1002/jor.1100140225

Wagnieres, G. A., Star, W. M., & Wilson, B. C. (1998). In vivo fluorescence spectroscopy and imaging for oncological applications. *Photochemistry and Photobiology*, *68*(5), 603–632. https://doi.org/10.1111/j.1751-1097.1998.tb02521.x

Wang, H. W., Lin, Y. C., Pai, T. W., & Chang, H. T. (2011). Prediction of B-cell linear epitopes with a combination of support vector machine classification and amino acid propensity identification. *Journal of Biomedicine & Biotechnology*, *2011*, 432830.

Wang, Z., Weitzmann, M. N., Sangadala, S., Hutton, W. C., & Yoon, S. T. (2013). Link protein N-terminal peptide binds to bone morphogenetic protein (BMP) type II receptor and drives matrix protein expression in rabbit intervertebral disc cells. *The Journal of Biological Chemistry*, *288*(39), 28243–28253. https://doi.org/10.1074/jbc.M113.451948

Woessner, J. F. Jr. (1961). The determination of hydroxyproline in tissue and protein samples containing small proportions of this imino acid. *Archives of Biochemistry and Biophysics*, *93*, 440–447. https://doi.org/10.1016/0003-9861(61)90291-0

Yankelevich, D. R., Ma, D., Liu, J., Sun, Y., Sun, Y., Bec, J., … Marcu, L. (2014). Design and evaluation of a device for fast multispectral time-resolved fluorescence spectroscopy and imaging. *The Review of Scientific Instruments*, *85*(3), 034303. https://doi.org/10.1063/1.4869037

Yu, W., Liu, T., Valdez, R., Gwinn, M., & Khoury, M. J. (2010). Application of support vector machine modeling for prediction of common diseases: The case of diabetes and pre-diabetes. *BMC Medical Informatics and Decision Making*, *10*, 16–16. https://doi.org/10.1186/1472-6947-10-16

Zhang, L., Hu, J., & Athanasiou, K. A. (2009). The role of tissue engineering in articular cartilage repair and regeneration. *Critical Reviews in Biomedical Engineering*, *37*(1–2), 1–57. https://doi.org/10.1615/CritRevBiomedEng.v37.i1-2.10

Zhou, X., Haudenschild, A. K., Sherlock, B. E., Hu, J. C., Leach, J. K., Athanasiou, K. A., & Marcu, L. (2018). Detection of glycosaminoglycan loss in articular cartilage by fluorescence lifetime imaging. *Journal of Biomedical Optics*, *23*, 1–8. https://doi.org/10.1117/1.JBO.23.12.126002

Zhu, W., Lai, W. M., & Mow, V. C. (1991). The density and strength of proteoglycan-proteoglycan interaction sites in concentrated solutions. *Journal of Biomechanics*, *24*(11), 1007–1018. https://doi.org/10.1016/0021-9290(91)90018-I

SUPPORTING INFORMATION

Additional supporting information may be found online in the Supporting Information section at the end of the article.

Figure S1. Representative stress relaxation curve from compression testing. The time-dependent stress results from a steady 10% strain from 0 to 600s immediately followed by a 20% strain from 600 to 1500s for tissue engineered neocartilage.

Figure S2. Exogenous LOXL2 enhances the coefficient of viscosity. The coefficient of viscosity A) increased with +LOX treatment and B) showed a moderate correlation with FLIm CH1 LT.

Figure S3. Exogenous LOXL2 treatment alters tissue thickness. LOXL2 treatment significantly reduced sample thickness of tissue engineered neocartilage as compared to control and LINK treatment groups ($p < 0.001$). Average ± standard deviation ($n = 6$ per group).

How to cite this article: Haudenschild AK, Sherlock BE, Zhou X, et al. Non-destructive detection of matrix stabilization correlates with enhanced mechanical properties of self-assembled articular cartilage. *J Tissue Eng Regen Med*. 2019;1–12. https://doi.org/10.1002/term.2824